Quantum interference of pseudospin-1 fermions

Adesh Singh and Gargee Sharma

School of Physical Sciences, Indian Institute of Technology Mandi, Mandi 175005, India

Quantum interference is studied in a three-band model of pseudospin-1 fermions in the $\alpha - \mathcal{T}_3$ lattice. We derive a general formula for magnetoconductivity that predicts a rich crossover between weak localization (WL) and weak antilocalization (WAL) in various scenarios. Recovering the known results for graphene ($\alpha = 0$), we remarkably discover that WAL is notably enhanced when one deviates slightly from the graphene lattice, i.e., when $\alpha > 0$, even though Berry's phase is no longer π; this is attributed to the presence of multiple Cooperon channels. Upon further increasing α, a crossover to WL occurs that is maximal for the case of the Dice lattice ($\alpha = 1$). Our work distinctly underscores the role of nontrivial band topology in the localization properties of a two-dimensional lattice.

The interference of waves is so fundamental to physics that it unites various branches, including but not limited to optics, acoustics, quantum mechanics, solids, and cold atoms. In solids, if the disorder is sufficiently high, wave interference can lead to a complete suppression of electronic transport. This phenomenon is known as Anderson localization (AL) [1]. A precursor to AL, weak localization (WL) refers to the negative quantum correction to the Drude conductivity due to the interference of electron waves [2,3]. In WL theory, the deviation to the conductivity is expanded in terms of the parameter λ_F / l (λ_F and l being the Fermi wavelength and the mean free path, respectively). Since disorder is inevitable in nature, WL is the standard method to measure the phase coherence length as well as determine the relevant processes responsible for electron scattering [4,5]. Coupling the electrons to the magnetic field introduces a finite phase difference between the interfering waves, and hence, magnetoconductivity is a critical tool in the study of WL. In contrast to conventional WL, the presence of spin-orbit coupling can lead to phase shift via spin precession resulting in destructive interference of electron waves, thereby enhancing the conductivity. This phenomenon, termed weak antilocalization [6] (WAL), also occurs in Dirac and Weyl materials where pseudospin replaces the actual spin [7–17].

The Dirac and Weyl equations that originated in particle physics now describe the low-energy physics of materials such as graphene, Weyl semimetals, and van der Waals structures, leading to their resurgence in condensed matter physics [18–20]. The band topology of these materials makes them of high interest, which leads to peculiar properties. For instance, the presence of π Berry phase leads to the WAL effect in graphene [7–9]. Recent experimental breakthroughs in van der Waals heterostructures, such as the discovery of twisted bilayer graphene exhibiting flat bands, have further intensified research in this arena [21].

Almost all the quantum interference studies in these materials so far have been typically based on a two-band model that mimics Dirac and Weyl physics. Specifically, it was pointed out in the two-band Dirac fermion that a crossover from weak antilocalization to weak localization occurs as the π Berry phase reduces to zero with the inclusion of Dirac mass [14]. The problem of quantum interference effects on localization properties in multiband models is largely unexplored, despite the prevalence of such systems in solid-state experiments as well as cold atoms. For instance, the $\alpha - \mathcal{T}_3$ lattice model [22] that synthesizes the Dirac and flat-band physics in a single model comprises a hexagonal lattice with atoms situated at the vertices of the hexagons and their centers, thus describing a three-band system of pseudospin-1 fermions [Fig. 1(f)]. By varying the hopping parameter between two sublattices, one interpolates between graphene ($\alpha = 0$) and the dice lattice ($\alpha = 1$). The $\alpha - \mathcal{T}_3$ model can be realized in trilayers of cubic lattices, $Hg_{1-x}Cd_xTe$ quantum wells, and cold-atom systems [23–26].

In this work, we solve the problem of quantum interference in pseudospin-1 fermions and examine the localization properties of electrons in the $\alpha - \mathcal{T}_3$ lattice, deriving a general formula for magnetoconductivity that predicts a rich crossover between localization and antilocalization in various scenarios. We first recover the known results for graphene ($\alpha = 0$). For the case of only elastic impurities, we remarkably discover that weak antilocalization is notably enhanced when one deviates slightly from the graphene lattice (i.e., when $\alpha > 0$), even though Berry's phase is no longer π. We attribute this behavior to the presence of two Cooperon channels. Upon further increasing α, we cross over to weak localization that is maximal for the case of Dice lattice ($\alpha = 1$). Since the band structure is independent of α, our model distinctly highlights the role of nontrivial band topology in the localization properties of electrons confined to the two-dimensional $\alpha - \mathcal{T}_3$ lattice.

We consider the following model of pseudospin-1 fermions in the $\alpha - \mathcal{T}_3$ lattice [22]:

$$H^\mu(\mathbf{k}) = \begin{pmatrix} 0 & a f_\mu(\mathbf{k}) & 0 \\ a f_\mu^*(\mathbf{k}) & 0 & b f_\mu(\mathbf{k}) \\ 0 & b f_\mu^*(\mathbf{k}) & 0 \end{pmatrix}, \qquad (1)$$
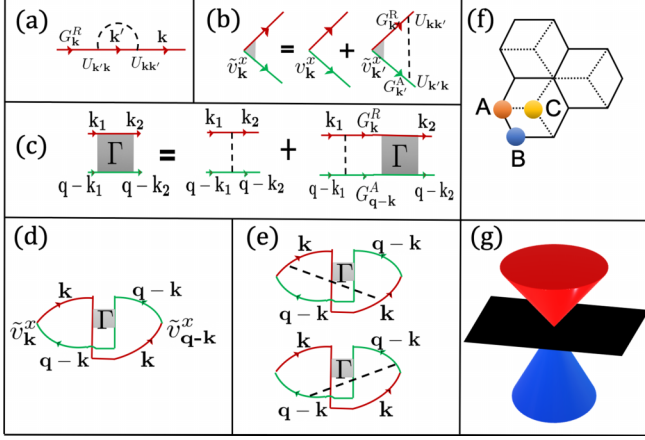
FIG. 1. (a) The retarded Green's function. (b) Vertex correction to the velocity. (c) The Bethe-Salpeter equation for the vertex. (d) Bare and (e) two dressed Hikami boxes for calculation of conductivity. (f) The $\alpha - \mathcal{T}_3$ lattice. The hopping between sublattices A and B, and A and C is t and αt, respectively. (g) The band structure of the $\alpha - \mathcal{T}_3$ lattice model with a flat band in the middle intersecting the Dirac cones.

where $f_\mu(\mathbf{k}) = \mu \hbar v_F(k_x - ik_y)$, $\mu = \pm 1$ is the valley index, v_F is the velocity parameter, $\psi = \tan^{-1}(\alpha)$ with $a = \cos \psi$, $b = \sin \psi$. The energy dispersion is given by $\epsilon_\mathbf{k} = 0, +\hbar v_F k$, and $-\hbar v_F k$, corresponding to a flat zero-energy band intersecting the linearly dispersing Weyl cone [Fig. 1(g)]. We focus on the case when the Fermi level intersects the conduction band, in which case the corresponding eigenfunction is given by $\psi_\mathbf{k}(\mathbf{r}) = (1/\sqrt{2})[\mu a e^{-i\mu\phi}, 1, \mu b e^{i\mu\phi}]e^{i\mathbf{k}\cdot\mathbf{r}}$.

We consider both elastic and (pseudo)magnetic impurities such that the impurity potential is given by $U(\mathbf{r}) = U_0(\mathbf{r}) + U_m(\mathbf{r})$, where $U_0(\mathbf{r})$ represents the elastic scattering potential and $U_m(\mathbf{r})$ the magnetic scattering potential. We assume pointlike disorder with $U_0(\mathbf{r}) = \sum_{\mathbf{R}_i} u_0^i S_0 \delta(\mathbf{r} - \mathbf{R}_i)$, $U_m(\mathbf{r}) = \sum_{\mathbf{R}_i} \sum_{\alpha=x,y,z} u_\alpha^i S_\alpha \delta(\mathbf{r} - \mathbf{R}_i)$, where we sum over impurity potentials located at random positions $\mathbf{R}_i$, $S_0 \equiv \mathbb{I}_3$, $\mathbf{S} = (S_x, S_y, S_z)$ is the vector of spin-1 matrices, and $u_{0,\alpha}^i$'s are the corresponding impurity potentials [27]. While comparing our results to the particular case of graphene ($a \to 1$), we must note that the spin matrices S_i's do not reduce to the two-component Pauli spin matrices σ_i's. For example, when $a \to 1$, the sublattice C is wholly decoupled, and while the S_z matrix couples with energy u_z to sublattice A and zero energy to sublattice B, different from a σ_z impurity where the coupling would be u_z to sublattice A and $-u_z$ to sublattice B. Thus when focusing on graphene with magnetic impurities, we must draw the comparison carefully, although we don't find qualitative differences in the results. We neglect the interference of different impurities with each other. In what follows, we assume in-plane isotropy ($u_x = u_y$), although, in Ref. [27], we also present results for the general case.

Quantum interference to conductivity in pseudospin-1 fermions is calculated diagrammatically [see Figs. 1(a)–1(e)]. The retarded (R) and advanced (A) Green's functions are $G_\mathbf{k}^{R/A}(\omega) = 1/(\omega - \epsilon_\mathbf{k} \pm i\hbar/2\tau)$, where the scattering rate is given by $\tau^{-1} = \tau_e^{-1} + \tau_z^{-1} + 2\tau_x^{-1}$; $\hbar\tau_e^{-1} = 2\pi N_F n_0 u_0^2(a^4 +$

$b^4 + 1)/4$ defines the elastic scattering rate, while $\hbar\tau_x^{-1} = 2\pi N_F n_m u_x^2/2$ and $\hbar\tau_z^{-1} = 2\pi N_F n_m u_z^2(a^4 + b^4)/4$ define the magnetic scattering rates. Furthermore, τ_e is related to the elastic scattering length ℓ_e by $\ell_e = \sqrt{D\tau_e}$, where $D = v_F^2 \tau/2$ is the diffusion constant. We similarly define the magnetic scattering lengths l_x and l_z as well. The vertex correction to the velocity [Fig. 1(b)] is evaluated by self-consistently solving the following equation: $\tilde{v}_\mathbf{k}^i = v_\mathbf{k}^i + \sum_{\mathbf{k}'} G_{\mathbf{k}'}^R G_{\mathbf{k}'}^A \langle U_{\mathbf{k},\mathbf{k}'} U_{\mathbf{k}',\mathbf{k}} \rangle_{\text{imp}} \tilde{v}_{\mathbf{k}'}^i$, where $\tilde{v}_\mathbf{k}^i = \eta_v v_\mathbf{k}$, and η_v is evaluated to be [27]

$$\eta_v^{-1} = 1 - [\alpha_e/(a^4 + b^4 + 1) + 2ab\alpha_x]. \tag{2}$$

We recover $\eta_v = 2$ for graphene [7,9]. The net conductivity is evaluated by summing over the contribution of one bare and two dressed Hikami boxes [Figs. 1(d) and 1(e)] [27]:

$$\sigma = -\frac{e^2 N_F \tau^3 \eta_v^2 v_F^2}{\hbar^2}(1 + 2\eta_H) \sum_\mathbf{q} \Gamma(\mathbf{q}), \tag{3}$$

where $N_F = E_F/2\pi(\hbar v_F)^2$ is the density of states, $\eta_H = -(1/2)(1 - \eta_v^{-1})$, and the vertex $\Gamma(\mathbf{q})$ is evaluated by solving the Bethe-Salpeter equation $\Gamma_{\mathbf{k}_1,\mathbf{k}_2} = \Gamma_{\mathbf{k}_1,\mathbf{k}_2}^0 + \sum_\mathbf{k} \Gamma_{\mathbf{k}_1,\mathbf{k}}^0 G_\mathbf{k}^R G_{\mathbf{q}-\mathbf{k}}^A \Gamma_{\mathbf{k},\mathbf{k}_2}$, where $\mathbf{q} = \mathbf{k}_1 + \mathbf{k}_2$. We recover $\eta_H = -1/4$ for graphene. In the limit when $\mathbf{q} \to 0$, the bare vertex is evaluated to be $\Gamma_{\mathbf{k}_1,\mathbf{k}_2}^0 \equiv \langle U_{\mathbf{k}_1,\mathbf{k}_2} U_{-\mathbf{k}_1,-\mathbf{k}_2} \rangle_{\text{imp}} = (\hbar/2\pi N_F \tau) \sum_m \sum_n z_{mn} e^{im\phi_1} e^{in\phi_2}$, where both m and n run between -2 and $+2$, and z_{mn} are entries of the matrix z given by [27]

$$z = \begin{pmatrix} 0 & 0 & 0 & 0 & z^{(-22)} \\ 0 & 0 & 0 & z^{(-11)} & 0 \\ 0 & 0 & z^{(00)} & 0 & 0 \\ 0 & z^{(1-1)} & 0 & 0 & 0 \\ z^{(2-2)} & 0 & 0 & 0 & 0 \end{pmatrix}, \tag{4}$$

and the elements are given by $z^{(-22)} = \frac{b^4 \alpha_e}{a^4 + b^4 + 1} + \frac{b^4 \alpha_z}{a^4 + b^4}$, $z^{(-11)} = \frac{2b^2 \alpha_e}{a^4 + b^4 + 1} - 2b^2 \alpha_x$, $z^{(00)} = \frac{(2a^2 b^2 + 1)\alpha_e}{a^4 + b^4 + 1} - \frac{2a^2 b^2 \alpha_z}{a^4 + b^4} - 4ab\alpha_x$, $z^{(1-1)} = \frac{2a^2 \alpha_e}{a^4 + b^4 + 1} - 2a^2 \alpha_x$, and $z^{(2-2)} = \frac{a^4 \alpha_e}{a^4 + b^4 + 1} + \frac{a^4 \alpha_z}{a^4 + b^4}$.

The Bethe-Salpeter equation [Fig. 1(c)] is solved using the ansatz $\Gamma_{\mathbf{k}_1,\mathbf{k}_2} = (\hbar/2\pi N_F \tau) \sum_m \sum_n \gamma^{mn} e^{im\phi_1} e^{in\phi_2}$, where the coefficients γ^{mn} of the matrix γ are solved by the equation $\gamma = (I - z\Phi)^{-1} z$, and $\Phi^{mn} = \frac{1}{2\pi} \int_0^{2\pi} e^{i(m+n)\phi}(1 + i\tau\mathbf{q}\cdot\mathbf{v}_F)^{-1} d\phi$. We evaluate [27]

$$\gamma^{(-mm)} = \frac{2\prod_{p\neq m} g^{(-pp)}}{\prod_k \left[g^{(-kk)} + Q^2\left(\sum_l \frac{1}{g^{(-ll)}} + \sum_q \frac{1}{g^{(-qq)}g^{(-q-1,q+1)}}\right)\right]}, \tag{5}$$

where the "Cooperon gaps" have been introduced $g^{(-ii)} = 2(1 - z^{(-ii)})/z^{(-ii)}$, and $Q = qv_F\tau$. Equation (5) along with Eq. (3) form the main results of this paper. We evaluate the vertex $\Gamma(\mathbf{q})$ retaining Cooperon gaps that result in diverging contributions to the conductivity [27].

The conductivity is evaluated by integrating Eq. (3) between $1/l_e$ and $1/l_\phi$ [7]. In the presence of a magnetic field, the wave vector q is quantized as $q_n^2 = (n + 1/2)4eB/\hbar$, where n is the Landau-level index. Summing over n and

TABLE I. Coefficients Σ_i^ϑ, $\mathcal{G}_i^\vartheta$, and ϕ_i^ϑ for graphene (g), dice (d), $\alpha - \mathcal{T}_3$ with elastic impurities (o), and $\alpha - \mathcal{T}_3$ with magnetic impurities in the z direction (z).

φ_0^g	1	φ_0^d	1	φ_0^o	-1	φ_0^z	1
Σ_0^g	$(g^{(1-1)})^{-1}$	Σ_0^d	$(g^{(-11)})^{-1}$	Σ_0^o	$(g^{(00)})^{-1}$	Σ_0^z	0
$\mathcal{G}_0^g$	$g^{(2-2)}$	$\mathcal{G}_0^d$	$g^{(00)}$	$\mathcal{G}_0^o$	$g^{(1-1)}$	$\mathcal{G}_0^z$	$g^{(2-2)}$
φ_1^g	-1	φ_1^d	0	φ_1^o	1	φ_1^z	1
Σ_1^g	$(g^{(00)})^{-1} + (g^{(2-2)})^{-1}$	Σ_1^d	0	Σ_1^o	$(g^{(1-1)})^{-1} + (g^{(-11)})^{-1}$	Σ_1^z	0
$\mathcal{G}_1^g$	$g^{(1-1)}$	$\mathcal{G}_1^d$	0	$\mathcal{G}_1^o$	$g^{(00)}$	$\mathcal{G}_1^z$	$g^{(-22)}$
φ_2^g	0	φ_2^d	0	φ_2^o	-1	φ_2^z	0
Σ_2^g	0	Σ_2^d	0	Σ_2^o	$g^{(00)}$	Σ_2^z	0
$\mathcal{G}_2^g$	0	$\mathcal{G}_2^d$	0	$\mathcal{G}_2^o$	$g^{(-11)}$	$\mathcal{G}_2^z$	0

subtracting the zero-field conductivity gives us magnetoconductivity $\Delta\sigma(B)$ [3]. We present magnetoconductivity results focusing on the weak-B regime, i.e., $l_B^2 \gg l_e^2$, and specifically focus on four special cases: graphene, dice lattice, and the $\alpha - \mathcal{T}_3$ with either elastic impurities or magnetic impurities in the z direction. We evaluate the following general expression for magnetoconductivity [27]:

$$\Delta\sigma(B) = \frac{e^2}{\pi h} \sum_{i=0}^{s_\vartheta} \alpha_i^\vartheta \left[\Psi\left(\frac{\ell_B^2}{\ell_\phi^2} + \frac{\ell_B^2}{\left(\ell_i^\vartheta\right)^2} + \frac{1}{2} \right) - \ln\left(\frac{\ell_B^2}{\ell_\phi^2} + \frac{\ell_B^2}{\left(\ell_i^\vartheta\right)^2} \right) \right], \quad (6)$$

where Ψ is the digamma function, $\vartheta \in \{g, d, o, z\}$ indicates graphene (g), dice (d), $\alpha - \mathcal{T}_3$ with elastic impurities (o), and $\alpha - \mathcal{T}_3$ with magnetic impurities in the z direction (z), and

$$\alpha_i^\vartheta = \frac{\varphi_i^\vartheta \left(\eta_v^\vartheta\right)^2 \left(1 + 2\eta_H^\vartheta\right)}{2\left(1 + \Sigma_i^\vartheta\right)}, \quad \left(\ell_i^\vartheta\right)^{-2} = \frac{\mathcal{G}_i^\vartheta}{2\ell^2\left(1 + \Sigma_i^\vartheta\right)}, \quad (7)$$

where $l^{-2} = l_e^{-2} + l_z^{-2} + 2l_x^{-2}$. The values of the coefficients Σ_i^ϑ, $\mathcal{G}_i^\vartheta$, and ϕ_i^ϑ are presented in Table I.

In the case of graphene ($a = 1$), the Cooperon gaps that can vanish are $g^{(1-1)}$, which results in WAL and $g^{(2-2)}$ that results in WL. We observe a crossover from weak localization to weak antilocalization as α_e varies from zero to unity. Magnetic impurities suppress WAL in graphene, as expected [14]. We plot this behavior in Fig. 2(a). Note that the other solution of
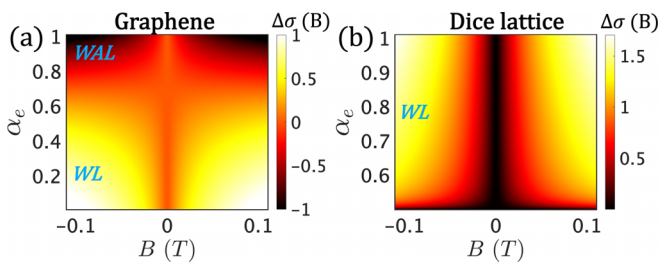
graphene ($a = 0$) is similar; the Cooperon gaps that vanish are $g^{(-11)}$, which results in WAL and $g^{(-22)}$ that causes WL.

In the case of dice lattice ($a = 2^{-\frac{1}{2}}$), the only vanishing Cooperon gap is $g^{(00)}$, which causes WL. In contrast to graphene lattice, dice lattice displays only weak localization, as seen in Fig. 2(b). This can be understood as the quantized Berry phase changes from π to zero as we change the hopping parameter from $a = 1$ (graphene) to $a = 2^{-\frac{1}{2}}$ (dice lattice).

In the presence of only elastic impurities ($\alpha_e = 1$), the Cooperon gaps that vanish are $g^{(1-1)}$, $g^{(-11)}$, both of which are WAL channels, and $g^{(00)}$, which is a WL channel. In Fig. 3(a) we plot the corresponding magnetoconductivity as a function of the parameter a. When $a = 0$ we observe WAL, as expected for graphene. Remarkably, as the parameter a is increased, WAL is notably enhanced even though the Berry phase decreases from its peak value π at $a = 0$. As the parameter a is increased to $2^{-\frac{1}{2}}$, WAL gradually crosses over to WL. The $\alpha \to \alpha^{-1}$ duality of the $\alpha - \mathcal{T}_3$ is reflected in the weak (anti)localization as a is increased beyond $2^{-\frac{1}{2}}$. The notable enhancement in WAL is attributed to the presence of two WAL channels ($g^{(-11)}$ and $g^{(1-1)}$) when $0 < a < 1$. We estimate that WAL is maximum when $a = 1/4$ or when $a = \sqrt{3}/2$.

In the presence of only magnetic S_z impurities ($\alpha_z = 1$), the Cooperon gaps $g^{(-22)}$ and $g^{(2-2)}$ yield the diverging contributions. In Fig. 3(b) we plot the corresponding magnetoconductivity. We observe WL throughout that attains its
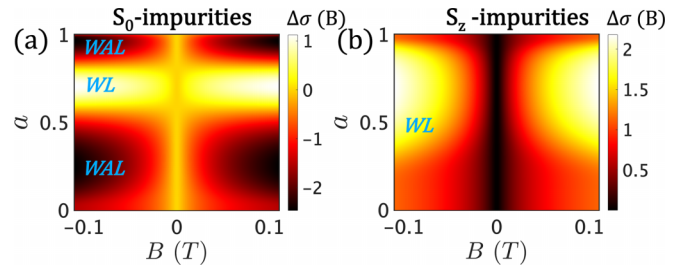

FIG. 2. Magnetoconductivity in the units of $e^2/\pi\hbar$. (a) Crossover from weak localization to weak antilocalization in graphene as α_e is increased, i.e., the relative scattering rate of the elastic impurities is increased compared to magnetic impurities. (b) Dice lattice displays only weak localization. We chose $l_\phi = 300$ nm and $l_e = 1000$ nm.

FIG. 3. Magnetoconductivity in the units of $e^2/\pi\hbar$. (a) Crossover from WAL ($a = 0$, graphene) to WL ($a = 2^{-\frac{1}{2}}$, dice) to WAL ($a = 1$, graphene) for elastic impurities ($\alpha_e = 1$). WAL is maximum slightly away from the graphene lattice, while WL is maximum for the dice lattice. (b) WL for the case of only S_z impurities. We chose $l_\phi = 300$ nm and $l_e = l_z = 1000$ nm.

maximum value for the dice lattice. For only S_x impurities (i.e., $\alpha_x = 1/2$), no diverging contributions to the Cooperon channels are obtained, and hence we do not discuss this case here.

In the $\alpha - \mathcal{T}_3$ Hamiltonian, when $\alpha = 0$ (hexagonal graphene lattice), the Hamiltonian belongs to the symplectic AII Wigner-Dyson class [28], similar to a spin-orbit coupled two-dimensional electron gas (2DEG). The in-plane spin-momentum locking necessitates (pseudo)spin-flip for quasiparticle backscattering. The sum of incoming and outgoing (pseudo)spins becomes zero, leading to the weak antilocalization from the Cooperon mode. For an arbitrary value of $\alpha \in (0, 1)$, time-reversal (TR) symmetry is still preserved, and thus the system belongs to the orthogonal Wigner-Dyson AI class. In general, such a system is similar to the conventional 2DEG and would show weak localization. Thus interpolating the value of α from zero to unity would result in smooth crossover from WAL to WL as shown earlier. In general, if the TR symmetry is microscopically broken, there would be a crossover to the unitary class where both WL and WAL are suppressed due to cancellation of time-reversed

electron interference paths. We speculate that trigonal warping effects may suppress WAL at higher densities, but time-reversal symmetry will tend to restore WL due to intervalley scattering [9]. Detailed analysis of trigonal warping and intervalley scattering is reserved for future studies.

In summary, quantum interference of electrons confined in the two-dimensional $\alpha - \mathcal{T}_3$ lattice can result in strikingly different localization-antilocalization properties, which can be manipulated by controlling the hopping strength of the electrons as well by magnetic doping. We derived a general formula for magnetoconductivity and predicted a rich crossover between weak localization and weak antilocalization in various different scenarios. We recovered the known results for graphene ($\alpha = 0$), we discovered that WAL is notably enhanced when the lattice is deviated slightly from the usual graphene lattice, i.e., when the Berry's phase is no longer π. We attributed this behavior to the presence of multiple Cooperon channels. Our work not only makes an important advance in the study of electron transport in two-dimensional materials but also will significantly drive experimental studies in cold atoms.

[1] P. W. Anderson, Absence of diffusion in certain random lattices, Phys. Rev. **109**, 1492 (1958).

[2] B. L. Altshuler, D. Khmel'Nitzkii, A. I. Larkin, and P. A. Lee, Magnetoresistance and Hall effect in a disordered two-dimensional electron gas, Phys. Rev. B **22**, 5142 (1980).

[3] G. Bergmann, Weak localization in thin films: A time-of-flight experiment with conduction electrons, Phys. Rep. **107**, 1 (1984).

[4] S. Chakravarty and A. Schmid, Weak localization: The quasiclassical theory of electrons in a random potential, Phys. Rep. **140**, 193 (1986).

[5] C. Beenakker and H. van Houten, Quantum transport in semiconductor nanostructures, in *Solid State Physics*, Vol. 44 (Elsevier, New York, 1991), pp. 1–228.

[6] S. Hikami, A. I. Larkin, and Y. Nagaoka, Spin-orbit interaction and magnetoresistance in the two dimensional random system, Prog. Theor. Phys. **63**, 707 (1980).

[7] H. Suzuura and T. Ando, Crossover from symplectic to orthogonal class in a two-dimensional honeycomb lattice, Phys. Rev. Lett. **89**, 266603 (2002).

[8] D. V. Khveshchenko, Electron localization properties in graphene, Phys. Rev. Lett. **97**, 036802 (2006).

[9] E. McCann, K. Kechedzhi, V. I. Fal'ko, H. Suzuura, T. Ando, and B. L. Altshuler, Weak-localization magnetoresistance and valley symmetry in graphene, Phys. Rev. Lett. **97**, 146805 (2006).

[10] R. V. Gorbachev, F. V. Tikhonenko, A. S. Mayorov, D. W. Horsell, and A. K. Savchenko, Weak localization in bilayer graphene, Phys. Rev. Lett. **98**, 176805 (2007).

[11] X. Wu, X. Li, Z. Song, C. Berger, and W. A. de Heer, Weak antilocalization in epitaxial graphene: Evidence for chiral electrons, Phys. Rev. Lett. **98**, 136801 (2007).

[12] F. V. Tikhonenko, D. W. Horsell, R. V. Gorbachev, and A. K. Savchenko, Weak localization in graphene flakes, Phys. Rev. Lett. **100**, 056802 (2008).

[13] G. Tkachov and E. M. Hankiewicz, Weak antilocalization in HgTe quantum wells and topological surface states: Massive versus massless Dirac fermions, Phys. Rev. B **84**, 035444 (2011).

[14] H.-Z. Lu, J. Shi, and S.-Q. Shen, Competition between weak localization and antilocalization in topological surface states, Phys. Rev. Lett. **107**, 076801 (2011).

[15] H.-Z. Lu, W. Yao, D. Xiao, and S.-Q. Shen, Intervalley scattering and localization behaviors of spin-valley coupled Dirac fermions, Phys. Rev. Lett. **110**, 016806 (2013).

[16] H.-Z. Lu and S.-Q. Shen, Finite-temperature conductivity and magnetoconductivity of topological insulators, Phys. Rev. Lett. **112**, 146601 (2014).

[17] B. Fu, H.-W. Wang, and S.-Q. Shen, Quantum interference theory of magnetoresistance in Dirac materials, Phys. Rev. Lett. **122**, 246601 (2019).

[18] A. H. C. Neto, F. Guinea, N. M. R. Peres, K. S. Novoselov, and A. K. Geim, The electronic properties of graphene, Rev. Mod. Phys. **81**, 109 (2009).

[19] S. D. Sarma, S. Adam, E. H. Hwang, and E. Rossi, Electronic transport in two-dimensional graphene, Rev. Mod. Phys. **83**, 407 (2011).

[20] N. P. Armitage, E. J. Mele, and A. Vishwanath, Weyl and Dirac semimetals in three-dimensional solids, Rev. Mod. Phys. **90**, 015001 (2018).

[21] Y. Cao, V. Fatemi, S. Fang, K. Watanabe, T. Taniguchi, E. Kaxiras, and P. Jarillo-Herrero, Unconventional superconductivity in magic-angle graphene superlattices, Nature (London) **556**, 43 (2018).

[22] A. Raoux, M. Morigi, J.-N. Fuchs, F. Piéchon, and G. Montambaux, From dia- to paramagnetic orbital susceptibility of massless fermions, Phys. Rev. Lett. **112**, 026402 (2014).

[23] F. Wang and Y. Ran, Nearly flat band with Chern number $C = 2$ on the dice lattice, Phys. Rev. B **84**, 241103(R) (2011).

[24] M. Rizzi, V. Cataudella, and R. Fazio, Phase diagram of the Bose-Hubbard model with $\mathscr{T}_3$ symmetry, Phys. Rev. B **73**, 144511 (2006).

[25] J. D. Malcolm and E. J. Nicol, Magneto-optics of massless Kane fermions: Role of the flat band and unusual Berry phase, Phys. Rev. B **92**, 035118 (2015).

[26] E. Serret, P. Butaud, and B. Pannetier, Vortex correlations in a fully frustrated two-dimensional superconducting network, Europhys. Lett. **59**, 225 (2002).

[27] See Supplemental Material at http://link.aps.org/supplemental/10.1103/PhysRevB.108.195426 for all the technical details of the calculations.

[28] F. J. Dyson, The threefold way, Algebraic structure of symmetry groups and ensembles in quantum mechanics, J. Math. Phys. **3**, 1199 (1962).